

SDC-Net: A Domain Adaptation Framework with Semantic-Dynamic Consistency for Cross-Subject EEG Emotion Recognition

Jiahao Tang[†], Youjun Li[†], Xiangting Fan, Yangxuan Zheng, Siyuan Lu, Xueping Li, Peng Fang, Chenxi Li* and Zi-Gang Huang*

Abstract—Electroencephalography(EEG) based emotion recognition holds great promise for affective brain-computer interfaces (aBCIs), yet practical deployment remains challenging due to substantial inter-subject variability and the lack of labeled data in target domains. To overcome these limitations, we present a novel unsupervised Semantic-Dynamic Consistency domain adaptation network for fully label-free cross-subject EEG emotion recognition. First, we introduce a Same-Subject Same-Trial Mixup strategy that generates augmented samples via intra-trial interpolation, enhancing data diversity while explicitly preserving individual identity to mitigate label ambiguity. Second, we construct a dynamic distribution alignment module in reproducing kernel Hilbert space (RKHS), jointly aligning marginal and conditional distributions through multi-objective kernel mean embedding, and leveraging a confidence-aware pseudo-labeling strategy to ensure stable adaptation. Third, we propose a dual-domain similarity consistency learning mechanism that enforces cross-domain structural constraints based on latent pairwise similarities, enabling semantic boundary learning without relying on temporal synchronization or label priors. To validate the effectiveness and robustness of the proposed SDC-Net, extensive experiments are conducted on three widely used EEG benchmark datasets: SEED, SEED-IV, and Faced. Comparative results against existing unsupervised domain adaptation methods demonstrate that SDC-Net achieves state-of-the-art performance in emotion recognition under both cross-subject and cross-session conditions. This advancement significantly improves the accuracy and generalization capability of emotion decoding, and lays a solid foundation for real-world applications of personalized affective brain-computer interfaces (aBCIs). The source code will be released at <https://github.com/XuanSuTrum/SDC-Net>.

Index Terms—affective brain-computer interfaces, emotion recognition, electroencephalogram, domain adaptation, individual variability, transfer learning, Hilbert Space Embeddings

I. INTRODUCTION

*Corresponding author: ChenXi Li and Zi-Gang Huang

[†] These authors contributed equally to this work.

This work was supported by the Natural Science Foundation of China (No. 11975178), Natural Science Basic Research Program of Shaanxi (No. 2023JC-YB-07).

Jiahao Tang, Youjun Li, Xiangting Fan, Yangxuan Zheng, Siyuan Lu and Zi-Gang Huang are affiliated with the Institute of Health and Rehabilitation Science, School of Life Science and Technology, Xi'an Jiaotong University, as well as the Research Center for Brain-Inspired Intelligence, Xi'an Jiaotong University. Chenxi Li and Peng Fang are affiliated with Department of Military Medical Psychology, Fourth Military Medical University, Xi'an, 710032, PR China. Military Medical Psychology School, Fourth Military Medical University, Xi'an, People's Republic of China. Xueping Li is affiliated with School of Automation and Information Engineering, Xi'an University of Technology, Xi'an, China

EMOTION play a pivotal role in human experience, reflecting the complex and dynamic interplay between physiological states and neural activity. Understanding the mechanisms underlying emotion generation, perception, and regulation is critical for advancing mental health interventions and enhancing human-computer interaction systems [1]. Against this backdrop, electroencephalography (EEG)-based emotion recognition has attracted considerable attention in affective computing due to its non-invasiveness and high temporal resolution [2], [3]. EEG signals capture rapid neural dynamics associated with emotional states, offering a valuable window into the underlying mechanisms of emotional processing. Furthermore, decoding emotion-related EEG patterns lays the theoretical foundation for developing emotion-aware brain-computer interfaces (BCIs) and adaptive human-centric systems.

Despite its promising potential, EEG-based emotion recognition still faces two primary challenges. First, EEG signals exhibit significant inter-subject variability and intra-subject non-stationarity, severely limiting the generalizability of recognition models across individuals. Second, acquiring high-quality emotion labels requires complex experimental protocols and substantial manual effort, which constrains the scalability of labeled datasets. These issues hinder the real-world deployment of EEG-based emotion recognition systems. Therefore, it is crucial to develop label-efficient and subject-robust recognition frameworks.

Transfer learning offers a compelling solution to these challenges by utilizing knowledge from a labeled source domain to boost performance in an unlabeled target domain [4]. In EEG-based emotion recognition, the source domain typically consists of labeled EEG recordings from multiple subjects, while the target domain comprises unlabeled EEG signals [5]. Transfer learning, particularly domain adaptation (DA), holds great potential to mitigate inter-subject variability by aligning distributions between domains and transferring learned representations from D_s to D_t [6].

Existing state-of-the-art DA methods for EEG-based emotion recognition can be broadly categorized into three paradigms. The first line of work enforces consistency constraints at the output or feature level to improve cross-domain generalization. Representative approaches include multi-source feature extraction [7], [8], adversarial feature alignment (e.g., DANN [9]), and pseudo-label propagation strategies [10]. While effective in aligning distributions, these

approaches often ignore the semantic structure between instances and are prone to noisy pseudo-labels, particularly under unsupervised target settings. To further improve the discriminative capacity of the learned features, a second category of methods introduces structural modeling techniques, such as pairwise or triplet loss constraints [11]–[14] and prototype-based representations. These methods typically guide target samples toward pre-learned emotion category prototypes in the source domain, treating them as “semantic anchors.” However, due to distributional shifts, these anchors may become misaligned in the target domain, leading to suboptimal guidance and reduced transfer performance. More recently, contrastive learning has gained popularity for learning subject-invariant and emotion-discriminative representations by maximizing agreement between samples from the same emotional state and minimizing it across different states [15]–[18]. Nevertheless, most contrastive frameworks rely on temporally synchronized experimental protocols to define positive and negative pairs, which implicitly leverage label information and limit their applicability in real-world unsupervised scenarios.

Despite recent advances, current methods in cross-subject EEG emotion recognition still face three fundamental challenges. First, although data augmentation strategies—such as GAN-based generation or cross-subject sample mixing [19]–[21]—aim to alleviate the scarcity of EEG data by increasing data diversity, they often fail to reduce label ambiguity. Second, most domain adaptation frameworks rely on static or shallow distribution alignment techniques, which are insufficient to model the evolving discrepancies between marginal and conditional distributions in high-dimensional EEG feature spaces. This limitation results in poor generalization and unstable adaptation performance across heterogeneous subjects. Third, existing contrastive learning and similarity-based methods typically depend on temporally synchronized experimental protocols or pseudo-label assumptions to construct positive and negative sample pairs. These dependencies implicitly introduce supervisory signals, contradicting the assumption of fully unsupervised learning and limiting their applicability in real-world, asynchronous, or spontaneous emotional scenarios. Moreover, in the absence of reliable guidance, these methods struggle to capture fine-grained semantic boundaries in the target domain, leading to increased class ambiguity and reduced discriminability.

To address the aforementioned challenges, we propose a novel domain adaptation framework for cross-subject EEG emotion recognition, which systematically tackles individual variability, semantic structure modeling, and distribution alignment. The main contributions of this work are as follows:

(1) Same-Subject Same-Trial Mixup (SS-Mix): Inspired by the Mixup augmentation strategy, we design an intra-subject, intra-trial sample mixing mechanism to enhance data diversity while preserving individual-specific traits. This strategy effectively mitigates the ambiguity between subject-specific features and emotion labels.

(2) Dynamic Distribution Alignment in RKHS: We construct a unified kernel mean embedding framework that jointly aligns marginal and conditional distributions in a shared RKHS space. This objective is formulated as a multi-

objective optimization problem to adaptively balance subject-level (global) and emotion-level (semantic) alignment. A dynamic confidence-based mechanism is further introduced to progressively filter high-confidence pseudo-labeled samples, improving conditional alignment reliability and transfer robustness.

(3) Dual-Domain Similarity Consistency Learning(DSCL): We introduce a structure-aware constraint that enforces pairwise similarity consistency across both source and target domains, enabling the model to capture fine-grained semantic boundaries without relying on temporal synchronization. This enhances generalization to complex and unlabeled emotional scenarios.

Notations and descriptions used in this paper is shown in Table I.

TABLE I
NOTATIONS AND DESCRIPTIONS USED IN THIS PAPER.

| Notation | Description |
|--------------------------------------|---|
| $D_s = \{x_s^l, y_s^l\}_{i=1}^{n_s}$ | Source domain |
| $D_t = \{x_t^u\}_{j=1}^{n_t}$ | Target domain |
| x_s^l / x_t^u | Source/Target domain samples |
| y_s^l | Ground truth labels in the source domain |
| n_s | Number of source domain samples |
| n_t | Number of target domain samples |
| $f()$ | Feature extractor |
| \hat{y}_s^l | Predicted labels for source domain |
| \hat{y}_t^u | Pseudo labels for target domain |
| K | Gaussian Kernel function |
| $RKHS$ | Reproducing Kernel Hilbert Space |
| SGD | Stochastic Gradient Descent |
| $ReLU$ | Rectified Linear unit activation function |

II. RELATED WORK

A. EEG-Based Emotion Recognition and Deep Learning Approaches

Traditional EEG-based emotion recognition primarily relies on classical machine learning methods, which typically involve two separate stages: manual feature extraction followed by classification. These approaches depend heavily on hand-crafted features, thus requiring researchers to possess strong domain expertise to identify emotion-relevant neural patterns. However, when applied to large-scale and complex EEG datasets, such methods often suffer from limited scalability and poor generalization performance [22]–[24].

With the advancement of deep learning, significant progress has been made in EEG-based emotion recognition. In particular, architectures such as Convolutional Neural Networks (CNNs) and Bidirectional Long Short-Term Memory networks (BiLSTMs) have demonstrated strong capabilities in automatically extracting discriminative features from raw or minimally preprocessed EEG signals [25]. For instance, certain methods construct three-dimensional EEG representations by integrating spatial and spectral information across channels, enabling CNN-based models to achieve arousal and valence classification accuracies of 89.67% and 90.93%, respectively, on benchmark datasets [26]. Furthermore, hybrid architectures combining CNNs and BiLSTMs have been explored, which

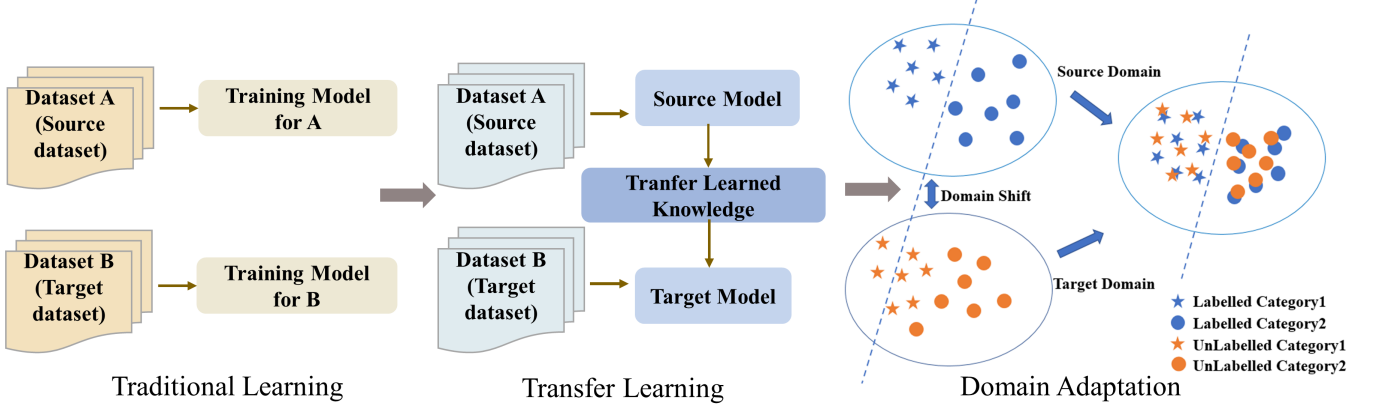


Fig. 1. Traditional machine learning models are trained in isolation on separate datasets, without benefiting from shared knowledge. Transfer learning bridges this gap by reusing the knowledge learned by a source model, trained on a source dataset, and applying it to a target dataset, thereby improving efficiency. Within transfer learning, domain adaptation specifically addresses domain shift, a scenario where the data distributions of D_s and D_t are misaligned. By aligning these distributional differences, domain adaptation methods enable models to perform robustly on D_t , even with minimal labeled data.

simultaneously capture the spatial structure and temporal dependencies in EEG signals, thereby enhancing emotion recognition performance [24].

Despite the promising performance of deep learning methods in within-subject emotion recognition tasks, their generalization to cross-subject and cross-session scenarios remains a critical challenge due to individual differences and temporal variability in EEG signals. This limitation significantly restricts the applicability of these models in real-world scenarios [27], [28].

B. Data Augmentation for EEG Emotion Recognition

Due to the scarcity and high acquisition cost of EEG signals, especially in emotion recognition tasks, recent work has turned to data augmentation (DA) techniques to improve model generalization. A representative line of research leverages generative adversarial networks (GANs) to synthesize high-quality EEG-like signals. For instance, GANSER [19] introduces a self-supervised GAN framework to generate diverse EEG samples by masking and regenerating partial inputs, thereby enriching the training distribution. Similarly, SA-cWGAN [20] incorporates self-attention to capture long-range dependencies in EEG signals and employs Wasserstein loss with gradient penalty to enhance sample fidelity, demonstrating notable gains on SEED and DEAP datasets. Du et al. [21] further propose L-C-WGAN-GP, which integrates LSTM-based generation with CNN-based discrimination, producing EEG signals that statistically resemble real distributions across frequency and time domains.

However, most GAN-based augmentation methods focus on enhancing sample quantity rather than preserving semantic consistency across individuals. These methods often neglect the intrinsic variability in emotional EEG responses across subjects, which can unintentionally exacerbate the inter-subject discrepancy. Moreover, direct synthetic sampling may distort class boundaries or introduce ambiguity between subject-specific features and emotional semantics.

C. Domain Adaptation Methods for Cross-Subject EEG Emotion Recognition

Electroencephalography (EEG) has been widely adopted in affective computing due to its high temporal resolution and direct access to cognitive and emotional states. However, the presence of significant inter-subject variability and inherent nonstationarity limits the generalization capability of emotion recognition models across individuals. To address this, DA techniques have been actively explored as effective strategies to transfer knowledge from labeled source domains to unlabeled or sparsely labeled target domains. A conceptual overview illustrating the differences among traditional learning, transfer learning, and domain adaptation in cross-domain EEG settings is presented in Fig. 1. This figure highlights the core challenges of distribution mismatch and label scarcity that domain adaptation aims to address. Building upon this framework, existing DA methods for EEG-based emotion recognition can be broadly categorized into three paradigms.

1) *Feature Alignment and Adversarial Methods:* A major line of DA research focuses on aligning feature distributions between domains to learn domain-invariant representations. Early approaches employed statistical alignment techniques or adversarial objectives to reduce marginal and conditional distributional shifts. For example, Chen et al. [7], and Li et al. [8] leveraged multi-source domain adaptation frameworks to extract both shared and domain-specific features. Adversarial strategies, such as DANN [9] and PR-PL [13], introduced domain discriminators trained jointly with the feature extractor to enforce domain confusion, promoting feature-level invariance. Additionally, pseudo-labeling and consistency regularization techniques have been adopted to refine target predictions in an unsupervised manner [10]. While these methods are effective in reducing global distribution discrepancies, they often lack mechanisms to model semantic relationships between instances, making them vulnerable to label noise and impairing their ability to delineate fine-grained emotional states.

2) *Similarity-based and Instance-level Methods:* To overcome the limitations of purely distribution-based alignment,

another line of research integrates structural modeling techniques to enhance the semantic discriminability of EEG features across domains. These methods typically incorporate metric-based constraints, such as pairwise or triplet losses, to enforce intra-class compactness and inter-class separability in the latent space [11], [12]. In addition, prototype-based methods utilize category centroids from the source domain as semantic anchors, encouraging target samples to align with these prototypical representations [13], [14]. While effective under moderate domain shift, this alignment often becomes unreliable in fully unsupervised settings due to the misalignment of prototypes caused by distributional discrepancies. Moreover, these approaches typically depend on accurate source label structures and can be sensitive to noisy or incorrect pseudo-labels when applied to unlabeled target domains.

Prototype-based methods treat the centroid of each emotion category in the source domain as a "semantic anchor" and encourage target samples to align with their nearest prototypes in the latent space. However, under domain shifts, these prototypes are prone to positional drift in the target domain, which undermines their effectiveness as guidance signals. Moreover, such methods rely heavily on accurate source label structures and are susceptible to noisy pseudo-labels when applied in low-label or fully unsupervised settings.

3) *Contrastive Learning Methods*: Contrastive learning has emerged as a powerful paradigm for learning discriminative and subject-invariant EEG representations in emotion recognition tasks without relying on explicit supervision. These methods typically construct positive and negative sample pairs based on the assumption that EEG signals elicited under the same emotional stimuli should be mapped closer in the feature space, while signals from different stimuli should remain apart. Shen et al. [15] proposed CLISA, which aligns inter-subject EEG representations using a contrastive objective, treating samples from the same video as positive pairs. Similarly, Dai et al. [16] incorporated spatial constraints across brain areas to generate region-aware contrastive pairs, improving intra-region consistency. Hu et al. [17] extended this idea by computing cross-subject correlations in temporal, spatial, and frequency domains, aligning representations using a correlation-based contrastive loss. Wang et al. [18] introduced GC-STCL, which employed Granger causality to enhance spatial-temporal structure learning in contrastive settings.

Despite achieving promising results, most of these methods define contrastive pairs based on temporally synchronized protocols—such as subjects watching the same video simultaneously—which implicitly encode label-related information. This contradicts the assumptions of fully unsupervised learning and limits generalizability in real-world, asynchronous, or spontaneous emotional environments. Moreover, their reliance on temporal alignment or external synchronization protocols constrains their applicability in more naturalistic or deployment settings.

III. METHODOLOGY

As illustrated in Fig. 2, the proposed SDC-Net framework is designed to address the challenges of cross-subject EEG

emotion recognition under fully label-free conditions. The overall pipeline begins with EEG data augmentation and feature extraction (Fig. 2a), where we introduce a SS-Mix strategy to improve the diversity and robustness of input samples. This augmentation is performed independently on both source and target domains, ensuring that subject-specific traits are preserved while mitigating overfitting caused by limited data. The augmented EEG signals are then passed through a shared feature extractor to obtain high-level representations. To reduce the domain discrepancy between source and target subjects, we propose a dynamic distribution alignment mechanism in RKHS (Fig. 2b). Specifically, we jointly align the marginal and conditional distributions using MMD and CMMMD, formulated as a multi-objective optimization problem. A dynamic thresholding strategy is further applied to progressively select high-confidence pseudo-labeled target samples, improving the reliability of conditional alignment and enhancing transfer robustness. Finally, to capture fine-grained semantic relationships beyond global alignment, we introduce a DSCL strategy (Fig. 2c). This component enforces structure-aware similarity consistency between paired samples across domains by aligning pairwise distances in both feature and label spaces. Importantly, this strategy does not rely on temporal synchronization, allowing the model to generalize effectively to complex and unlabeled emotional scenarios. Together, these components form a unified and fully unsupervised domain adaptation framework tailored for robust EEG-based emotion recognition across subjects.

A. Data augmentation and Feature Extractor

1) *EEG data augmentation Based SS-Mix*: The Mixup method performs data augmentation by creating convex combinations of pairs of samples, which extends the distribution space of the training data to a certain extent and enhances the model's generalization capability. This simple yet effective method [29] has been proven to possess unique advantages in improving model robustness and reducing overfitting.

The mathematical expression for Mixup can be represented as follows:

$$\tilde{x} = \omega x_i + (1 - \omega) x_j \quad (1)$$

$$\tilde{y} = \omega y_i + (1 - \omega) y_j \quad (2)$$

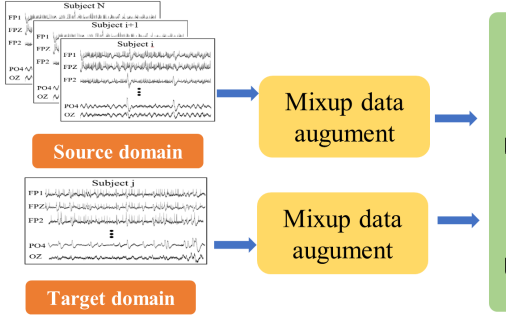
where (x_i, y_i) and (x_j, y_j) are two examples drawn at random from the training data, and λ is a random variable drawn from a Beta distribution (α, α) . α is a hyperparameter that controls the strength of the interpolation.

Based on the aforementioned approach, we further refined the data augmentation strategy by individually extracting and augmenting data from the same subject and the same trial, rather than augmenting all data together. This method better preserves individual differences across trials within each subject and ensures that the augmented samples maintain consistency and physiological relevance.

Specifically, we segmented each subject's dataset into different trials and applied the Mixup method separately to each trial. Within each trial, sample pairs were augmented as follows:

$$\tilde{x}_{trial} = \omega x_{trial}^i + (1 - \omega) x_{trial}^j \quad (3)$$

a EEG Data Augmentation and Feature Extractor



c Dual-Domain Similarity Consistency Learning Strategy

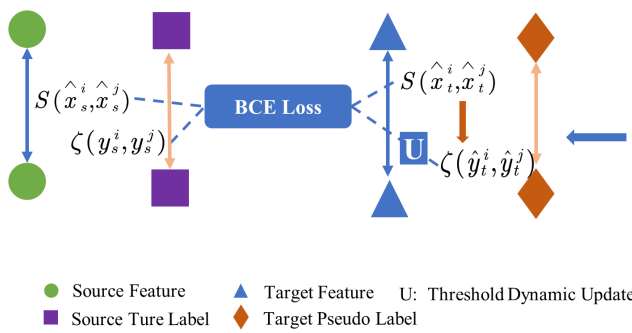


Fig. 2. The flowchart of the proposed SDC-Net framework.

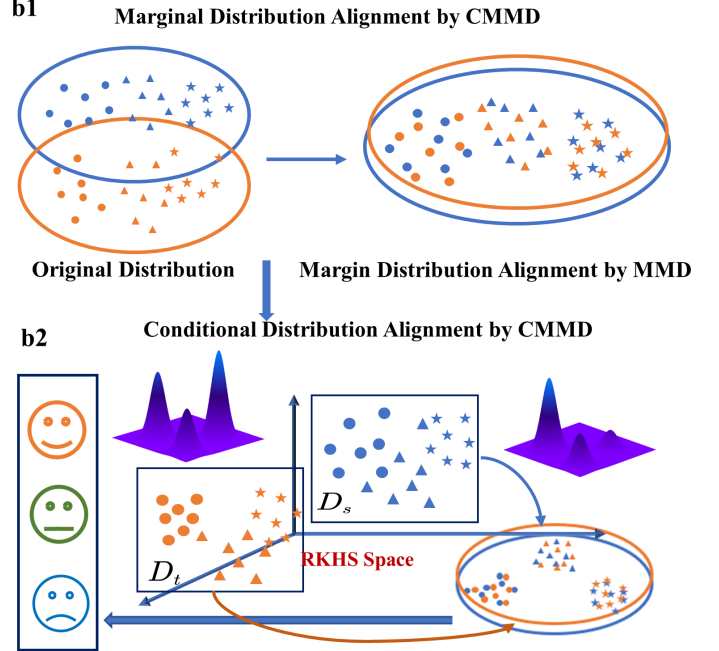
$$\tilde{y}_{trial} = \omega y_{trial}^i + (1 - \omega) y_{trial}^j \quad (4)$$

Here, x_{trial}^i and x_{trial}^j are two randomly selected samples within the same trial, y_{trial}^i and y_{trial}^j are their corresponding labels. Unlike global data augmentation, this method ensures the consistency of data within trials while further enhancing the preservation of individual differences during the augmentation process. This approach not only expands the distributional space of the data but also minimizes potential physiological and psychological differences between subjects that could interfere with model training. Consequently, it enhances the model's generalization capability and robustness in cross-subject emotion recognition tasks.

2) *Feature Extractor*: In the domain of EEG signal analysis, a rigorous feature extraction process was implemented to distill meaningful information from the raw EEG data. The procedure began with the careful selection of specific time segments from the EEG signal, aiming to capture temporal information relevant to the analysis. Following this, the short-time Fourier transform (STFT) was employed to decompose the EEG signal into its constituent frequency bands: delta (δ), theta (θ), alpha (α), beta (β), and gamma (γ) bands. This decomposition allowed for the isolation and examination of different frequency components, each of which is associated with distinct neurological and cognitive processes.

Within each frequency band, the probability density function (PDF) of the signal amplitude was calculated. The PDF

b Semi-supervised Domain Adaptation with Dynamic Distribution Alignment Network



provides a statistical representation of the distribution of signal amplitudes within each frequency band, offering insights into the underlying characteristics of the EEG signal.

The central aspect of this feature extraction process is the computation of differential entropy, a measure that quantifies the uncertainty and complexity of the EEG signal. Differential entropy is a continuous analog of the discrete Shannon entropy and is defined as:

$$H(x) = - \int p(x) \log p(x) dx \quad (5)$$

In Eq.(5), $H(X)$ represents the differential entropy of the random variable x , which in this context corresponds to the amplitude of the EEG signal. The function $p(x)$ denotes the probability density function of the amplitude distribution within a given frequency band. The differential entropy $H(X)$ thus provides a scalar measure of the unpredictability or information content inherent in the EEG signal within that specific frequency band.

This feature extraction process was systematically applied to each frequency band, computing differential entropy values for each individual band. As a result, each EEG sample is represented by a differential entropy feature vector of dimension $N_{cf} = c \times f$, where c denotes the number of EEG channels and $f = 5$ corresponds to the number of frequency bands. This representation effectively captures the spectral-spatial characteristics of the EEG signals, providing

a robust and informative foundation for further analysis and interpretation.

B. Dynamic Distribution Alignment in RKHS

To address the distributional discrepancy between source domain D_s and target domain D_t in EEG emotion recognition, we propose a unified framework named Dynamic Distribution Alignment in RKHS. This method performs joint alignment of MPD and CPD in a shared RKHS. The key idea is to unify marginal and conditional alignment into a single kernel mean embedding (KME)-based framework.

1) *Unified Alignment Framework*: Given a kernel function $k(x, x') = \langle \psi(x), \psi(x') \rangle$, the KME of a distribution $P(x)$ is:

$$\mu_P = \mathbb{E}_{x \sim P}[\psi(x)] \quad (6)$$

For a conditional distribution $P(x|y)$, the embedding is:

$$\mu_{X|y} = \mathbb{E}_{X|y}[\psi(X)] = M_{X|Y}\varphi(y) \quad (7)$$

where $M_{X|Y}$ is the conditional embedding operator, and $\varphi(y)$ denotes the label kernel feature. This leads to the following unified alignment objective:

$$\mathcal{L}_{\text{align}} = \mathbb{E}_{y \sim Y} \|\mu_{P(x|y)} - \mu_{Q(x|y)}\|_{\mathcal{H}}^2 \quad (8)$$

This unified objective naturally encompasses both marginal and conditional alignment scenarios. When label information is not considered and only the marginal distribution $P(x)$ is aligned, we obtain the standard MMD for aligning global feature distributions:

$$\mathcal{L}_{\text{MMD}} = \|\mu_{P(x)} - \mu_{Q(x)}\|_{\mathcal{H}}^2 \quad (9)$$

When class-conditional structures are taken into account, the objective becomes the CMMD, which aligns distributions conditioned on class labels.

$$\mathcal{L}_{\text{CMMD}} = \sum_{c=1}^C \|\mu_{P(x|y=c)} - \mu_{Q(x|y=c)}\|_{\mathcal{H}}^2 \quad (10)$$

2) *Alignment of Marginal Distribution Alignment In RKHS*: Given source domain samples $D_s = \{x_i^s\}_{i=1}^n$ and target domain samples $D_t = \{x_j^t\}_{j=1}^m$, the empirical MMD is computed as:

$$\begin{aligned} \mathcal{L}_{\text{MMD}} = & \frac{1}{n^2} \sum_{i,j=1}^n k(x_i^s, x_j^s) + \frac{1}{m^2} \sum_{i,j=1}^m k(x_i^t, x_j^t) \\ & - \frac{2}{nm} \sum_{i=1}^n \sum_{j=1}^m k(x_i^s, x_j^t) \end{aligned} \quad (11)$$

We adopt a multi-kernel Gaussian kernel to enhance robustness:

$$\begin{aligned} k(u, v) = & \sum_{l=1}^L \exp \left(-\frac{\|u - v\|^2}{\sigma_l} \right) \\ \sigma_l = & \sigma_0 \cdot \kappa^{l-L/2} \end{aligned} \quad (12)$$

where κ is the kernel multiplier, L is the number of Gaussian kernels, and σ_0 is the base bandwidth computed as the average squared pairwise distance between all samples. This formulation enables capturing similarities at multiple scales and improves the robustness of domain discrepancy estimation.

3) *Alignment of Conditional Probability Distributions In RKHS*: Most prior work on domain adaptation in EEG-based emotion recognition focuses on aligning marginal distributions between the source and target domains. However, aligning the CPDs, i.e., $P(x|y)$, is equally critical to ensure semantic consistency across domains. To address this, we adopt the CMMD framework, which measures the discrepancy between class-conditional distributions in a RKHS.

The CMMD loss is defined as:

$$\mathcal{L}_{\text{CMMD}} = \sum_{c=1}^C \|\mu_{P(x|y=c)} - \mu_{Q(x|y=c)}\|_{\mathcal{H}}^2 \quad (13)$$

where $\mu_{P(x|y=c)}$ and $\mu_{Q(x|y=c)}$ denote the KME of the conditional distributions from the source and target domains, respectively.

Since the target domain lacks ground-truth labels, we use pseudo-labels predicted by the classifier: $\hat{y}_t^u = f(x_t^u)$. Rather than estimating posteriors $P(y|x)$ and $Q(y|x)$ directly, we focus on sufficient statistics of the class-conditional distributions $P(x|y)$ and $Q(x|y)$.

In RKHS, the conditional mean embedding is expressed as Eq.7. The operator $M_{X|Y}$ can be constructed from the covariance operators:

$$M_{X|Y} = \mathcal{S}_{XY} \mathcal{S}_{YY}^{-1} \quad (14)$$

with the cross-covariance operator defined as:

$$\mathcal{S}_{XY} = \mathbb{E}_{XY}[\psi(X) \otimes \varphi(Y)] - \mathbb{E}_X[\psi(X)] \otimes \mathbb{E}_Y[\varphi(Y)] \quad (15)$$

where \otimes denotes the tensor product.

In practical settings, the conditional embedding operator can be estimated from m samples. Define the input and label feature matrices:

$$\Theta = [\psi(x_1), \dots, \psi(x_m)] \in \mathbb{R}^{d \times m}, \quad (16)$$

$$\xi = [\varphi(y_1), \dots, \varphi(y_m)] \in \mathbb{R}^{k \times m} \quad (17)$$

We compute the centered empirical cross-covariance:

$$\hat{S}_{XY} = \frac{1}{m} \Theta H \xi^{\top}, \quad H = I - \frac{1}{m} \mathbf{1} \mathbf{1}^{\top} \quad (18)$$

The estimated conditional embedding operator is then:

$$\hat{M}_{X|Y} = \Theta(\xi^{\top} \xi + \lambda I)^{-1} \xi^{\top} \quad (19)$$

where λ is a small regularization coefficient to ensure numerical stability.

Let the feature and label matrices from source and target domains be:

- Source domain: Θ_s , ξ_s , kernel matrices $K_s = \Theta_s^{\top} \Theta_s$, $\Upsilon_s = \xi_s^{\top} \xi_s$
- Target domain: Θ_t , ξ_t , kernel matrices $K_t = \Theta_t^{\top} \Theta_t$, $\Upsilon_t = \xi_t^{\top} \xi_t$
- Cross-domain: $K_{st} = \Theta_s^{\top} \Theta_t$, $\Upsilon_{ts} = \xi_t^{\top} \xi_s$

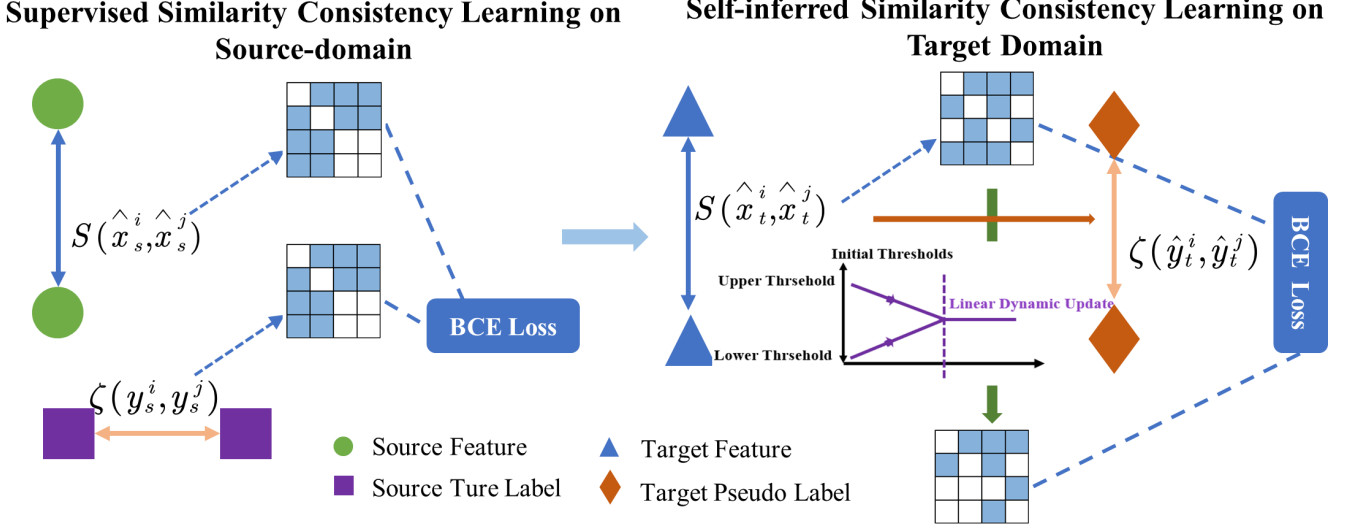


Fig. 3. The flowchart of the proposed SDC-Net framework.

Define regularized matrices:

$$\tilde{\Upsilon}_s = \Upsilon_s + \lambda I, \quad \tilde{\Upsilon}_t = \Upsilon_t + \lambda I$$

Then the CMMMD loss in matrix form becomes:

$$\begin{aligned} \hat{\mathcal{L}}_{\text{CMMMD}} = & \text{Tr} \left(\Upsilon_s \tilde{\Upsilon}_s^{-1} K_s \tilde{\Upsilon}_s^{-1} \right) + \text{Tr} \left(\Upsilon_t \tilde{\Upsilon}_t^{-1} K_t \tilde{\Upsilon}_t^{-1} \right) \\ & - 2 \cdot \text{Tr} \left(\Upsilon_{ts} \tilde{\Upsilon}_s^{-1} K_{st} \tilde{\Upsilon}_t^{-1} \right) \end{aligned} \quad (20)$$

To mitigate the effect of noisy pseudo-labels from the target domain, we adopt a dynamic confidence-based selection mechanism. Let \hat{y}_i^t denote the predicted label distribution for target sample x_i^t . If the confidence $\max(\hat{y}_i^t) \geq \tau$, the pseudo-label is accepted; otherwise, the sample is excluded from CMMMD computation. Formally:

$$\hat{D}_t = \{ \Gamma(p_i^u, \tau) \cdot \hat{y}_i^u \}_{i=1}^{N_u}, \quad \tau \in [0, 1] \quad (21)$$

The threshold τ increases over training to incorporate more reliable samples. The final CMMMD loss (Eq. 20) is computed only on high-confidence samples from \hat{D}_t to ensure robust conditional distribution alignment.

C. Dual-Domain Similarity Consistency Learning Strategy

To promote discriminative and transferable feature representations for EEG signals, we propose a DSCL strategy. This module encourages the learned feature space to maintain pairwise semantic consistency—ensuring that samples from the same class are closer, and those from different classes are further apart. It does so by applying pairwise similarity learning in both the source and target domains, as illustrated in Fig. 3.

1) Supervised Similarity Consistency on Source Domain:

In the source domain D_s , ground-truth labels are available, allowing us to supervise the model's feature similarity predictions. Given two source samples x_s^i and x_s^j with labels y_s^i and y_s^j , we define their true semantic similarity using a binary indicator:

$$\zeta(y_s^i, y_s^j) = \begin{cases} 1, & \text{if } y_s^i = y_s^j \\ 0, & \text{otherwise} \end{cases} \quad (22)$$

Their feature similarity is computed by cosine similarity over the normalized embeddings \hat{x}_s^i and \hat{x}_s^j :

$$S(\hat{x}_s^i, \hat{x}_s^j) = \frac{\hat{x}_s^i \cdot \hat{x}_s^j}{\|\hat{x}_s^i\| \cdot \|\hat{x}_s^j\|}, \quad S' = \frac{S+1}{2} \quad (23)$$

We map S to the $[0, 1]$ interval as S' , allowing it to be compared with the binary label using binary cross-entropy (BCE) loss. The supervised similarity loss is:

$$\mathcal{L}_{ps} = \frac{1}{N_s(N_s-1)} \sum_{i \neq j} l(\zeta(y_s^i, y_s^j), S'(\hat{x}_s^i, \hat{x}_s^j)) \quad (24)$$

where $l(\cdot)$ is the BCE loss. This objective enforces semantic structure preservation within the source domain, enhancing intra-class compactness and inter-class separation.

2) Self-Inferred Similarity Consistency on Target Domain:

In the target domain D_t , labels are unavailable. To still enable pairwise semantic learning, we utilize pseudo-labels \hat{y}_t generated from the model itself using the confidence-based filtering strategy (see Eq. ??).

The key idea is to *infer* pairwise relationships based on cosine similarity. For target feature embeddings \hat{x}_t^i and \hat{x}_t^j , we define:

$$\zeta(\hat{y}_t^i, \hat{y}_t^j) = \begin{cases} 1, & \text{if } S(\hat{x}_t^i, \hat{x}_t^j) \geq \tau_{pu} \\ 0, & \text{if } S(\hat{x}_t^i, \hat{x}_t^j) < \tau_{pl} \end{cases} \quad (25)$$

Here, τ_{pu} and τ_{pl} represent dynamic upper and lower thresholds used to determine confident positive or negative pairs, respectively. Feature similarities within the ambiguous region $[\tau_{pl}, \tau_{pu}]$ are excluded to avoid noisy supervision. These thresholds are linearly adjusted during training to gradually

include more pairs as the model becomes more confident (visualized in Fig. 3).

Only confident pairs $(i, j) \in \mathcal{P}$ are selected for learning, and the target-domain loss is:

$$\mathcal{L}_{pt} = \frac{1}{|\mathcal{P}|} \sum_{(i,j) \in \mathcal{P}} l\left(\zeta(\hat{y}_t^i, \hat{y}_t^j), S'(\hat{x}_t^i, \hat{x}_t^j)\right) \quad (26)$$

D. Loss Function and Training Procedure of SDC-Net

To enable robust domain adaptation under fully unlabeled target conditions, the proposed SDC-Net is optimized with a unified objective comprising five loss components: the classification loss on the source domain (\mathcal{L}_{Ds}), marginal and conditional distribution alignment losses (\mathcal{L}_{mmd} and \mathcal{L}_{cmmd}), and pairwise similarity losses on both the source (\mathcal{L}_{ps}) and target (\mathcal{L}_{pt}) domains. These components are integrated into the following total loss:

$$\mathcal{L} = \mathcal{L}_{Ds} + \alpha \mathcal{L}_{mmd} + \beta \mathcal{L}_{cmmd} + \beta \mathcal{L}_{pt} + \lambda \mathcal{L}_{ps} \quad (27)$$

The classification loss \mathcal{L}_{Ds} supervises the prediction of labeled source domain samples using cross-entropy, and is defined as:

$$\mathcal{L}_{Ds} = -\frac{1}{B_L} \sum_{i=1}^{B_L} \sum_{c=1}^C y_s^l(i, c) \log p_s^l(i, c) \quad (28)$$

where B_L is the batch size, C denotes the number of emotion classes, y_s^l is the one-hot ground-truth label, and p_s^l is the predicted probability distribution.

To bridge the distributional gap between domains, we employ both marginal and conditional alignment losses. The marginal distribution alignment is performed via MMD, while conditional alignment is handled through CMMMD, which utilizes high-confidence pseudo-labeled target samples. These two components guide the feature space toward domain invariance while preserving emotion-specific semantics.

In addition, to capture semantic structure, we impose similarity consistency constraints. The \mathcal{L}_{ps} loss leverages source labels to model intra-class and inter-class relations, while \mathcal{L}_{pt} promotes structural consistency on the target domain using high-confidence pseudo-labels. These losses enforce that samples from the same emotion class remain close in the latent space, even across domains.

To balance the influence of each loss component throughout training, we adopt a dynamic weighting strategy. The coefficient α begins with a high value to prioritize marginal alignment and is gradually reduced to emphasize semantic alignment in later stages. The coefficient β is adjusted based on the classification loss via a step function:

$$\beta = \varepsilon(\rho_0 - \mathcal{L}_{Ds}) + \frac{1}{2} \varepsilon(\mathcal{L}_{Ds} - \rho_0) \varepsilon(\rho_1 - \mathcal{L}_{Ds}) \quad (29)$$

where $\varepsilon(\cdot)$ is the Heaviside step function, and ρ_0 , ρ_1 are two predefined thresholds.

To further enhance semantic modeling on the target domain, the weight λ for the unsupervised pairwise loss \mathcal{L}_{pt} increases linearly with training epochs:

$$\lambda = \frac{2e}{\text{epochs}} \quad (30)$$

This progressive adjustment ensures that SDC-Net shifts from global alignment to finer semantic refinement as training evolves, ultimately improving generalization performance in fully unsupervised cross-subject EEG emotion recognition tasks. The overall learning process is detailed in Algorithm 1.

Algorithm 1 SDC-Net: Domain-Adaptive Representation Learning

Input: Source domain dataset $D_s = \{(x_s^l, y_s^l)\}_{i=1}^N$, Target domain dataset $D_t = \{x_t^u\}_{i=1}^{N_u}$, Percentile parameter α , Total epochs E

Output: Predicted labels for target domain D_t

- 1: **for** epoch $e = 1$ to E **do**
- 2: Sample interpolation weight $\omega \sim \text{Beta}(\alpha, \alpha)$. Augment trial data via convex combinations per Eqs. (3), (4).
- 3: Extract mini-batches $D_{\text{batch}}^s \subseteq D_s$ and $D_{\text{batch}}^t \subseteq D_t$ through random sampling.
- 4: Derive 310-dimensional EEG feature representations using short-time Fourier transform and differential entropy.
- 5: Compute MMD loss to align marginal distributions, as per Eq. (11).
- 6: Infer pseudo-labels $\hat{y}_t^u = f(x_t^u)$ and probability distributions p_i^u for $x_t^u \in D_{\text{batch}}^t$, addressing the absence of ground-truth labels in D_t .
- 7: Compute dynamic confidence threshold. Select high-confidence samples as per Eq. 21.
- 8: Evaluate CMMMD loss using \hat{D}_t per Eq. (20), and compute source domain cross-entropy loss per Eq. (28).
- 9: Calculate pairwise alignment losses for D_s and D_t using cosine similarity and thresholded pseudo-labels, as defined in Eqs. (24), (26).
- 10: Optimize network parameters by minimizing the composite loss \mathcal{L} with dynamically adjusted weights α , β , λ per Eqs. (27), (29), (30), via gradient descent.
- 11: **end for**
- 12: **return** Predicted labels for D_t .

IV. EXPERIMENTS

A. Emotion datasets

To demonstrate the effectiveness of our method, SDC-Net for cross-subject EEG-based emotion recognition, we conduct experiments on four public benchmark datasets: SEED, SEED-IV, and FACED.

In the SEED dataset, fifteen Chinese subjects participated in the experiments, with each subject completing three sessions, each consisting of a total of 15 trials. Throughout the experiments, participants were exposed to Chinese film clips specifically designed to elicit a spectrum of emotions, including positive, neutral, and negative states [30].

In the SEED IV dataset, a total of 15 subjects took part in the experiments. For each participant, three sessions were conducted on separate days, with each session comprising 24

trials. During each trial, the participant viewed one of several film clips designed to induce emotions such as happiness, sadness, neutrality, and fear. The EEG signals in both the SEED and SEED IV datasets were recorded using a 62-channel ESI NeuroScan System [31].

In the FACED dataset, a total of 123 Chinese participants took part in the experiments, each completing 28 trials. Four trials were conducted to elicit neutral emotions, while the remaining trials targeted various other emotions. The movie clips lasted between 34 and 129 seconds and were specifically selected to induce a range of emotions, including anger, fear, disgust, sadness, amusement, inspiration, joy, tenderness, and neutrality. During the emotion induction process, EEG signals were recorded using the NeuSen.W32 system (Neuracle, China) with 32 channels. Two types of classification tasks were performed on the FACED dataset: one for fine-grained discrete emotion classification (nine categories) and another for binary classification to distinguish between positive emotions (amusement, inspiration, joy, tenderness) and negative emotions (anger, fear, disgust, sadness) [32].

B. Implementation details

In the model presented in this paper, the feature extractor is composed of a pair of fully connected layers. The initial layer, denoted as "fc1," processes input data spanning 310 dimensions and reduces it to 64 dimensions using a ReLU activation function. Subsequently, the data flows through the second layer, labeled "fc2," further reducing the dimensionality to 64, accompanied by an additional ReLU activation. To optimize the model's performance and mitigate overfitting, dropout layers with a dropout rate of 0.25 are introduced after each fully connected layer. For the weight parameters of α , τ_h and τ_l are 1 and 0, respectively, while $\tau_m = \frac{2}{1+e^{-10 \cdot \frac{g}{200}}} - 1$, which is a logistic sigmoid-based function that transitions smoothly and tends to zero as the epoch progresses. For the Eq. (29), ρ_0 and ρ_1 are 0.1 and 0.15, respectively. The parameters τ_{pu} and τ_{pu} in pairwise learning are assigned values of 0.9 and 0.5, respectively.

For our experimental setup, we utilize all labeled source samples to represent the D_s , while the unlabeled target samples constitute the D_t . We evaluate and compare the average classification accuracy as a performance measure. Our training configuration encompasses several essential parameters and procedural steps. The batch size for training is set to 32, and the training process spans 200 epochs. We employ two distinct learning rates, specifically 0.001 and 0.01. The SGD momentum parameter is set to 0.9. Moreover, the option to enable or disable CUDA training is provided to the user. Additionally, we initialize a random seed value of 3 to ensure result reproducibility, and the L2 weight decay is precisely set at 5×10^{-4} . During training, we employ the SGD optimization method, with learning rates subject to dynamic adjustments at the beginning of each epoch. These adaptive changes in learning rates follow a specific mathematical formula. This iterative training process continues for the designated number of epochs, allowing the model to learn and adapt over time.

TABLE II
THE PERFORMANCE OF REPRESENTATION METHODS ON SEED DATASETS
USING CROSS-SUBJECT SINGLE-SESSION LEAVE-ONE-SUBJECT-OUT
CROSS-VALIDATION

| Method | Pcc(%) | Method | Pcc(%) |
|----------------|-------------------|-----------------|-----------------------------------|
| RGNN [33] | 85.30 \pm 06.72 | BiHDM [34] | 85.40 \pm 07.53 |
| JDA-Net [9] | 88.28 \pm 11.44 | DA-CapsNet [35] | 84.63 \pm 09.09 |
| MS-MDA [7] | 89.63 \pm 06.97 | WGAN-GP [36] | 87.10 \pm 07.10 |
| DGGN [37] | 83.84 \pm 10.26 | EPNNE [12] | 89.10 \pm 03.60 |
| DC-ASTGCN [38] | 80.65 \pm 08.46 | MS-FRAN [8] | 85.61 \pm 06.55 |
| SDDA [11] | 91.08 \pm 07.70 | CU-GCN [39] | 87.10 \pm 05.44 |
| DAPLP [10] | 89.44 \pm 04.89 | DS-AGC [40] | 86.38 \pm 07.25 |
| PR-PL [13] | 85.88 \pm 09.36 | PLMSDANet [41] | 84.21 \pm 12.34 |
| CLISA [15] | 86.40 \pm 06.40 | CL-CS [17] | 88.30 \pm 08.90 |
| ST-SCGNN [42] | 85.90 \pm 04.90 | SDC-Net | 91.85\pm05.98 |

C. Experiment Setting

In this study, the SEED and SEED_IV datasets were utilized as the foundational data sources for model training and evaluating the performance of cross-subject emotion detection. To comprehensively assess the effectiveness of the cross-subject emotion detection model, two distinct cross-validation methodologies were implemented. These methodologies aimed to provide a robust evaluation of the model's performance across different subjects.

Cross-Subject Single-Session Leave-One-Subject-Out Cross-Validation Results. This approach employs a widely embraced technique for cross-subject emotion detection using EEG signals. Specifically, a single-session leave-one-subject-out cross-validation strategy is employed. In our experiments, the EEG signals of each individual subject were designated as the D_t , while the data from all other subjects constituted the D_s . This process was systematically repeated, with each subject serving as the D_t in turn. The cross-subject average detection performance was then reported, providing a comprehensive evaluation of the approach's effectiveness.

Cross-Subject Cross-Session Leave-One-Subject-Out Cross-Validation Results. To comprehensively evaluate the model's performance across different sessions for each subject, we employed a cross-subject, cross-session leave-one-subject-out cross-validation method. In each experimental iteration, the complete session data of a specific subject was used as the D_t , while the sessions from all other subjects constituted the D_s . This iterative procedure ensured that each subject served as the D_t at least once, enabling the calculation of the average detection performance across subjects.

V. RESULT AND DISCUSSION

A. Experimental Results

1) Cross-subject single-session leave-one-out-subject-out cross-validation Results: In Tables II and III, we conducted a comprehensive evaluation of various representations on the SEED and SEED_IV datasets using the leave-one-subject-out cross-validation method with a cross-subject single-session protocol. Our method demonstrated significant performance advantages on the SEED dataset, achieving an accuracy of

TABLE III

THE PERFORMANCE OF REPRESENTATION METHODS ON SEED_IV DATASETS USING CROSS-SUBJECT SINGLE-SESSION LEAVE-ONE-SUBJECT-OUT CROSS-VALIDATION

| Method | Pcc(%) | Method | Pcc(%) |
|---------------|-------------------|----------------|-----------------------------------|
| DGCNN [43] | 68.73 \pm 08.34 | MS-STM [44] | 61.41 \pm 09.72 |
| MS-ADRT [45] | 68.98 \pm 06.80 | MS-MDA [7] | 59.34 \pm 05.48 |
| WGAN-GP [36] | 60.60 \pm 15.76 | JDA-Net [9] | 70.83 \pm 10.25 |
| ST-SCGCN [42] | 76.37 \pm 05.77 | CU-GCN [39] | 74.50 \pm 07.88 |
| DAPLP [10] | 74.57 \pm 06.18 | DS-AGC [40] | 66.00 \pm 07.93 |
| MSFR-GCN [46] | 73.43 \pm 07.32 | SDC-Net | 74.88\pm10.47 |

TABLE IV

PERFORMANCE COMPARISON OF METHODS ON FACED-2 AND FACED-9 DATASETS

| Method | FACED-2 (Pcc%) | FACED-9 (Pcc%) |
|-----------------------|-----------------------------------|-----------------------------------|
| DE+SVM [47] | 60.50 \pm 16.00 | 34.90 \pm 10.70 |
| DE+MLP [48] | 70.20 \pm 11.20 | 35.10 \pm 10.30 |
| DAN [49] | 53.40 \pm 07.10 | 37.20 \pm 09.10 |
| DANN [50] | 50.50 \pm 07.10 | 54.10 \pm 08.30 |
| CLISA [15] | 67.80 \pm 04.10 | 43.20 \pm 05.90 |
| GCPL [51] | / | 36.90 \pm 03.30 |
| CL-CS [17] | 72.50 \pm 15.30 | 43.40 \pm 13.70 |
| SDC-Net (Ours) | 75.20\pm08.46 | 42.40\pm06.55 |

91.85% \pm 05.98%. Similarly, on the SEED_IV dataset, our method exhibited competitive accuracy of 74.88% \pm 10.47%. These results strongly validate the substantial performance improvements achieved by our method on both datasets, particularly the remarkable accuracy of 91.85% \pm 05.98% on the SEED dataset, surpassing the industry average and demonstrating notable potential in the field of emotion recognition tasks. These findings provide compelling evidence supporting the effective application of our method in real-world scenarios.

As shown in Table IV, the SDC-Net model was evaluated on the FACED dataset for both binary classification of positive and negative emotions and nine-class emotion classification,

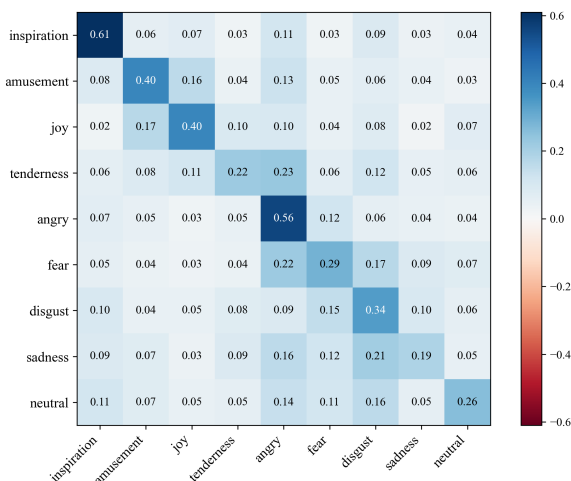


Fig. 4. The result of nine categories for Faced datasets.

TABLE V

THE PERFORMANCE OF SHARED METHODS ON SEED AND SEED_IV DATASETS USING CROSS-SUBJECT CROSS-SESSION LEAVE-ONE-SUBJECT-OUT CROSS-VALIDATION

| Method | SEED | SEED_IV |
|----------------|-----------------------------------|-----------------------------------|
| RF [52] | 69.60 \pm 07.64 | 50.98 \pm 09.20 |
| KNN [53] | 60.66 \pm 07.93 | 40.83 \pm 07.28 |
| SVM [54] | 68.15 \pm 07.38 | 51.78 \pm 12.85 |
| TCA [55] | 64.02 \pm 07.96 | 56.56 \pm 13.77 |
| CORAL [56] | 68.15 \pm 07.83 | 49.44 \pm 09.09 |
| SA [57] | 61.41 \pm 09.75 | 64.44 \pm 09.46 |
| GFK [58] | 66.02 \pm 07.59 | 45.89 \pm 08.27 |
| DANN [59] | 81.08 \pm 05.88 | 54.63 \pm 08.03 |
| SDC-Net | 82.22\pm04.68 | 68.84\pm08.05 |

achieving accuracies of 75.2% \pm 8.46% and 42.4% \pm 6.55%, respectively. Compared to the baseline model DE \pm SVM, it achieved improvements of and for the binary and nine-class tasks, respectively, highlighting the superior performance of our model, particularly in handling more fine-grained emotion classification tasks.

2) *Cross-subject cross-session leave-one-out-subject-out cross-validation results:* Another crucial consideration for emotion brain-computer interfaces is the substantial variability observed among different subjects across various sessions. The evaluation approach of cross-subject and cross-session represents a significant challenge for the effectiveness of models in EEG-based emotion recognition tasks. To further validate this detection approach, which aligns more closely with real-world application scenarios, we conducted experiments and obtained outstanding three-class classification performance on the SEED dataset, achieving an accuracy of 82.22% \pm 04.68% (see Table V). Additionally, on the SEED-IV dataset, our model achieved a four-class accuracy of 68.84% \pm 08.05% (see Table V). Compared to existing research, the proposed SDC-Net method demonstrated industry-leading performance with a smaller standard deviation. These results indicate that the proposed SDC-Net method exhibits excellent stability and generalization capabilities in handling subject and session differences.

B. Confusion matrices

In this section, we compare the performance of four different models: Da-CapsNet, PLMSDANet, LGDAAN-Net and our proposed model, SDC-Net, using confusion matrices (as shown in Fig. 2). The confusion matrices provide insight into how well each model classifies inputs into three categories: Negative, Neutral, and Positive. The diagonal elements represent correct predictions, while off-diagonal elements correspond to misclassifications. Our proposed SDC-Net model outperforms the other models, particularly in classifying the Neutral class with an accuracy of 92.45%, which is the highest among all models.

Additionally, SDC-Net achieves 95.7% accuracy in the Positive class and 87.23% in the Negative class. The confusion between classes is minimal, with only 5.25% of neutral instances being misclassified as negative and 2.53% of positive instances

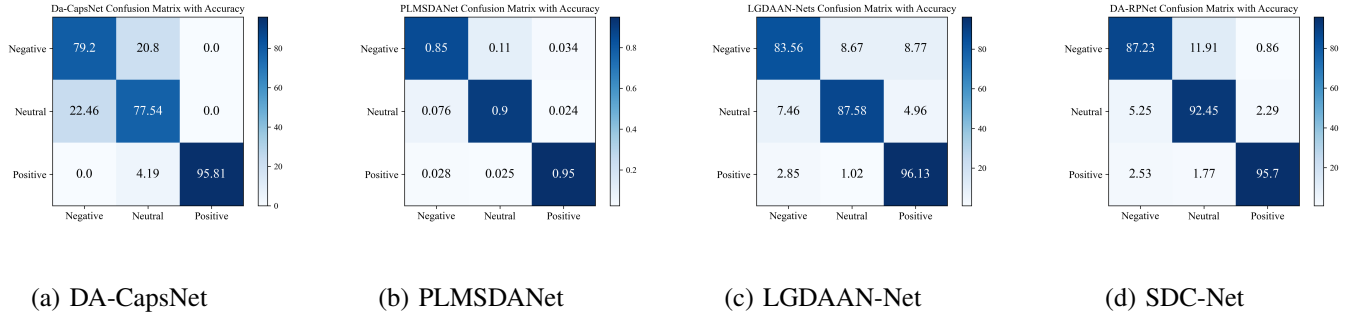


Fig. 5. Confusion matrices comparison: (a) DA-CapsNet [35], (b) PLMSDANet [41], (c) LGDAAN-Net [60], and (d) proposed SDC-Net. All subfigures share the same color scale for fair comparison.

being misclassified as negative. The low misclassification rates in SDC-Net suggest that our model effectively captures subtle differences between sentiment classes, particularly between negative and neutral sentiments, where other models faltered. It achieves the best accuracy in both the Neutral and Positive classes and exhibits significantly lower misclassification rates compared to the other models. This indicates that SDC-Net provides a more nuanced understanding of sentiment, making it particularly effective for tasks that require fine-grained sentiment analysis. In contrast, models like DA-CapsNet, despite excelling in classifying positive samples, demonstrate significant weaknesses in distinguishing negative and neutral sentiments, limiting their effectiveness in comprehensive sentiment classification tasks.

C. Ablation Study

To evaluate the contribution of each module in the proposed SDC-Net, we performed ablation experiments by systematically removing six key components. Table VI summarizes the performance under each setting in terms of average Pearson correlation coefficient (Pcc). First, domain alignment mechanisms were found to be essential. Removing the MMD component resulted in a significant drop in performance (86.82%), indicating its crucial role in reducing marginal distribution discrepancy between source and target domains. Similarly, excluding CMMd led to a moderate performance decline (89.91%), showing that conditional alignment further refines domain adaptation, though its impact is secondary to MMD. Second, the effect of DSCL was also prominent. Supervised similarity consistency on source domain contributes to extracting discriminative features from labeled source data, and its removal decreased the accuracy to 88.99%. More critically, excluding self-inferred similarity consistency learning on target domain reduced performance to 86.99%, emphasizing its importance in modeling intra-class similarity in the unlabeled target domain, thus supporting better generalization. Third, SS-Mix based data augmentation improved generalization by synthesizing diverse EEG trials. Its removal caused a noticeable decrease in Pcc (87.99%), suggesting its role in mitigating overfitting and increasing sample diversity. Finally, the pseudo-confidence mechanism, which filters unreliable pseudo-pairs, slightly improved the mean accuracy and significantly reduced variance. Without this mechanism, the model still achieved

TABLE VI
PERFORMANCE OF THE SDC-NET MODEL IN THE ABLATION STUDY

| Ablation Experiment Strategy | Pcc (%) |
|---|------------------------------------|
| without-SS-Mix | 87.99 ± 5.77 |
| without-mmd | 86.82 ± 5.86 |
| without-cmmd | 89.91 ± 5.03 |
| without-similarity consistency on D_s | 88.99 ± 6.06 |
| without-similarity consistency on D_t | 86.99 ± 5.65 |
| without-pseudo-confidence | 89.66 ± 7.18 |
| SDC-Net | 91.85 ± 5.98 |

89.66%, but with increased performance fluctuation (standard deviation 7.18), indicating its stabilizing effect on target domain predictions.

In summary, MMD and target similarity consistency learning are the most influential modules in our framework. The remaining components also enhance the model's robustness and consistency, contributing to the superior performance of SDC-Net across cross-subject EEG emotion recognition tasks.

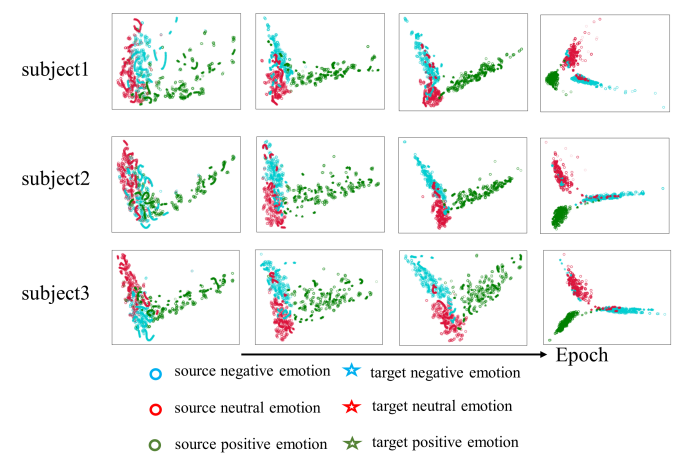


Fig. 6. t-SNE visualization of source and target domain emotion representations across training stages.

D. Visualization of Domain Alignment via t-SNE

To qualitatively assess the effectiveness of domain alignment, we visualized the feature distributions of source and

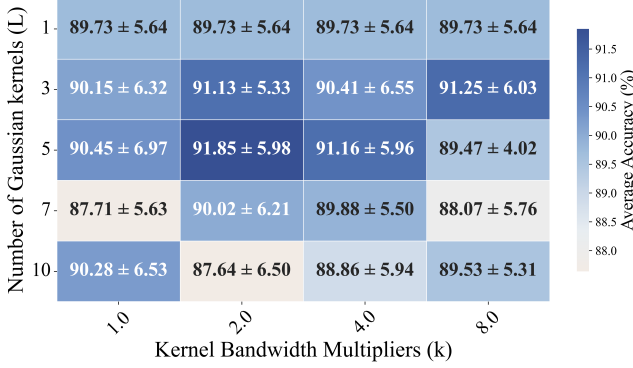


Fig. 7. Hyperparameter Analysis of the Multi-Scale Gaussian Kernel in RKHS-based Distribution Alignment.

target domains using t-SNE at different training stages (Fig. 6). In these plots, the source domain (D_s) is represented by circles and the target domain (D_t) by stars, with emotion categories indicated by color (blue: negative, red: neutral, green: positive). At the early training stage, features from D_s and D_t are poorly aligned. The target samples, especially for Subject 1 and Subject 2, are scattered and show significant overlap across emotion classes, indicating large domain discrepancy. Positive target samples (green stars) frequently overlap with other categories, suggesting the initial failure in feature alignment. As training progresses, domain alignment improves notably. For Subjects 2 and 3, the target domain emotion clusters begin to align with those of the source domain. Notably, negative and positive emotions become more separable, suggesting that MMD and CMMD modules effectively minimize marginal and conditional distribution gaps. By the final training stage, most emotion clusters exhibit clear separation in both domains. Subject 3 shows the most consistent alignment across categories, while Subject 1 retains partial overlap in neutral emotions. This aligns with known challenges in classifying neutral emotional states, which often lie closer to the decision boundaries due to their ambiguous EEG patterns.

Overall, the t-SNE visualizations provide intuitive support for the proposed framework’s ability to learn emotion-discriminative and domain-invariant features. Although some overlap remains—particularly for neutral states—the progressive clustering over epochs confirms the effectiveness of the domain adaptation strategy.

E. Sensitivity Analysis for Hyperparameters

1) *Gaussian Kernel Hyperparameters*: To evaluate the effect of kernel configuration on model performance, we analyze combinations of kernel number ($L \in 1, 3, 5, 7, 10$) and bandwidth multipliers ($\kappa \in 1, 2, 4, 8$). As shown in Fig. 7, increasing L from 1 to 5 consistently improves classification accuracy. The highest performance is achieved at $L = 5$, $\kappa = 2.0$ ($91.85\% \pm 5.98\%$), balancing local and global distribution alignment. However, using too many kernels ($L > 5$) introduces redundancy and noise, slightly degrading performance.

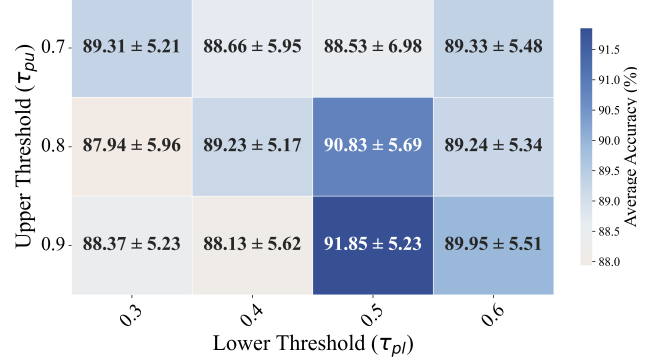


Fig. 8. Hyperparameter Analysis of Similarity Consistency Thresholds.

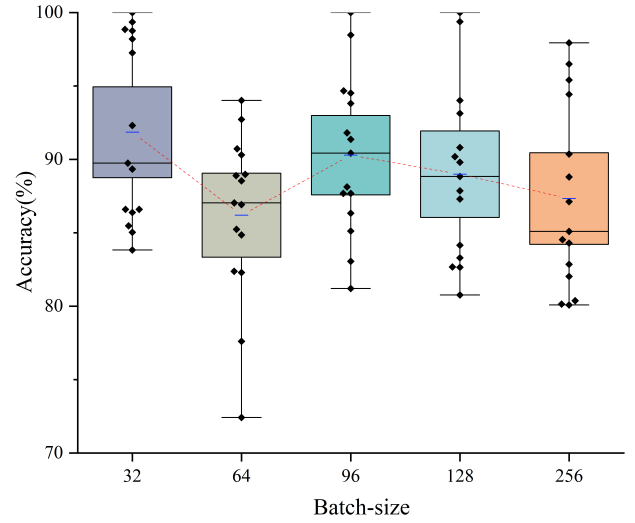


Fig. 9. Hyperparameter Analysis of Batch-Size.

Moderate bandwidth scaling ($\kappa = 2.0$) offers the best trade-off: small κ may overfit local variations, while large κ over-smooths inter-class differences. Overall, a small ensemble of Gaussian kernels with moderate scaling enables more effective representation alignment in RKHS.

2) *Effect of Similarity Consistency Thresholds*: We further examine the sensitivity of the similarity consistency mechanism by varying the upper and lower thresholds (τ_{pu}, τ_{pl}) used to define confident sample pairs in the target domain (see Fig. 8). The best performance ($91.85\% \pm 5.23\%$) is observed at ($\tau_{pu} = 0.9, \tau_{pl} = 0.5$), indicating that enforcing constraints only on highly confident pairs improves stability and accuracy. Narrow threshold gaps (e.g., (0.8, 0.6)) reduce the filtering of noisy relations, while looser settings (e.g., $\tau_{pl} = 0.3$) introduce more false dissimilarities. These results suggest that carefully calibrated thresholds are critical for filtering uncertainty and ensuring stable pairwise supervision.

3) *Effect of Batch-Size*: To investigate the influence of batch-size on model performance, we evaluate five different settings: 32, 64, 96, 128, and 256. As shown in Fig. 9, the model achieves the highest average accuracy when the batch-size is set to 32, with performance gradually degrading as

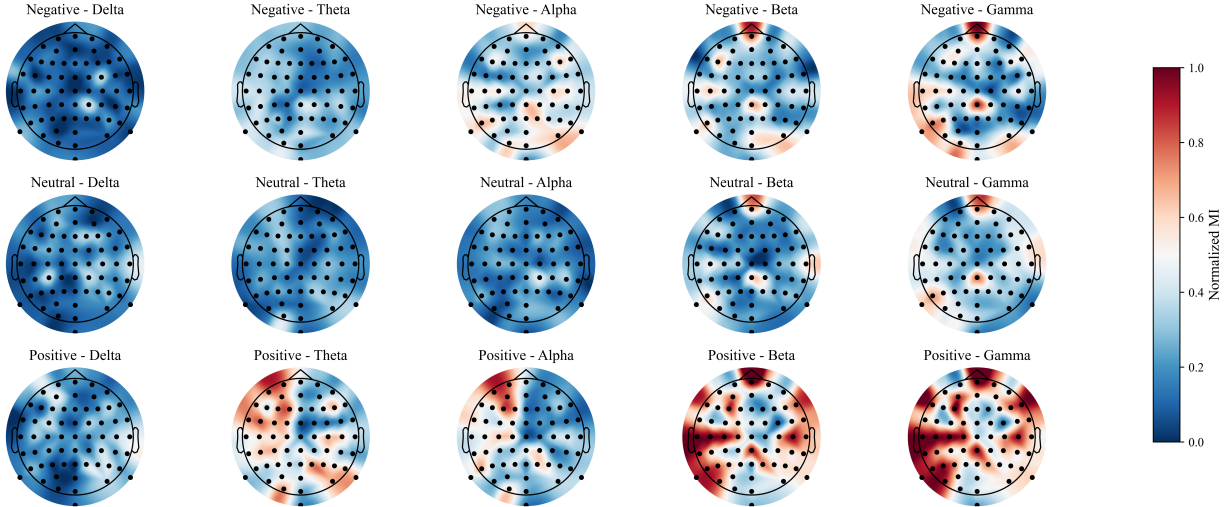


Fig. 10. Topographic analysis of the mutual information between the EEG patterns and the model predictions.

the batch-size increases. Notably, although batch-size = 64 and 96 still maintain relatively competitive results, large batch sizes (128 and 256) exhibit increased performance variance and a downward trend in mean accuracy. This phenomenon can be attributed to the trade-off between gradient estimation stability and generalization ability. Smaller batch sizes provide noisier but more generalizable gradient estimates, whereas larger batches lead to more stable updates but risk overfitting to dominant features. In our case, the batch-size of 32 strikes a better balance between convergence stability and generalization, yielding an average accuracy of 90.35% and a maximum of 100%. These findings suggest that an appropriately small batch-size is more beneficial for emotion-related EEG tasks, potentially due to the high variability and subject-specific nature of EEG signals.

F. Topographic Analysis of Important EEG Patterns

This study utilizes an EEG topographic mapping approach grounded in Mutual Information (MI) to evaluate the contributions of different brain regions and frequency bands to emotion classification. The preprocessed EEG feature matrix $X \in R^{N \times 5 \times 2}$, incorporating signals from 62 electrode channels across five frequency bands, is paired with the classification probability matrix $Y \in R^{N \times 3}$, corresponding to three emotional states: negative, neutral, and positive.

By computing the MI between each EEG feature and the predicted probabilities of the emotion categories, an initial MI $MI \in R^{3 \times 5 \times 2}$ tensor is derived, capturing the nonlinear statistical dependencies. This tensor is then normalized via min-max scaling to the $[0, 1]$ interval to enable fair comparison across dimensions.

The normalized MI scores are then structured into a three-dimensional tensor (emotion \times frequency band \times channel) and visualized topographically using the standard 10–20 system for electrode positioning. A 3×5 grid layout illustrates MI distributions across the Delta (1–4 Hz), Theta (4–8 Hz), Alpha (8–13 Hz), Beta (13–30 Hz), and Gamma (30–50 Hz) bands for each emotional category. Color gradients denote the

strength of feature importance, with electrode positions highlighted as black dots. This methodology effectively integrates information-theoretic metrics with neuroimaging visualization, offering intuitive insights into the spatial and spectral dynamics of emotion processing.

The results depicted in Fig.10 indicate that the most informative EEG patterns for emotion recognition are predominantly concentrated in the beta and gamma frequency bands within the frontal and temporal regions. These findings are consistent with prior research, reinforcing the role of high-frequency oscillations in affective processing [14], [43], [61].

TABLE VII
PERFORMANCE OF THE SDC-NET MODEL IN THE ABLATION STUDY

| Method | SEED | SEED_IV |
|----------------|----------|----------|
| PR-PL [13] | 1 | 3 |
| MS-MDA [7] | 3 | 8 |
| PLMSDANet [41] | 0 | 1 |
| SDC-Net | 0 | 0 |

G. Negative Transfer Results

This study evaluates the effectiveness of the proposed SDC-Net framework in alleviating negative transfer in fully unsupervised cross-subject EEG emotion recognition across 45 experimental tasks. Negative transfer is defined as a classification accuracy lower than 33.3% on the SEED dataset or 25% on the SEED_IV dataset. As shown in Table VII, SDC-Net achieved zero instances of negative transfer, demonstrating a clear advantage over conventional transfer learning approaches.

The robustness of SDC-Net in avoiding negative transfer can be attributed to three key components:(1)SS-Mix, which augments intra-subject data while preserving individual-specific characteristics, reducing ambiguity between subject identity and emotion labels;(2) Dynamic Distribution Alignment in RKHS, which jointly aligns marginal and class-conditional distributions using a unified kernel mean embedding framework, while adaptively filtering high-confidence

pseudo-labels to ensure alignment quality;(3) DSCL, which imposes structural constraints on pairwise similarities across domains, promoting semantic consistency without relying on temporal alignment. Together, these innovations enable SDC-Net to dynamically adjust to distribution shifts, suppress noisy pseudo-labels, and maintain semantic integrity across subjects, thereby ensuring stable and reliable transfer performance in complex, label-free EEG emotion recognition scenarios.

H. Why SDC-Net Works? Effectiveness Analysis

Addressing the significant inter-subject variability inherent in EEG data remains a central challenge in the development of robust and generalizable aBCI systems. In this work, we proposed SDC-Net, a novel semantic-dynamic consistency network, and conducted comprehensive evaluations on three publicly available affective EEG datasets: SEED, SEED-IV, and Faced. Experimental results consistently demonstrate that SDC-Net outperforms existing state-of-the-art methods in cross-subject emotion recognition tasks, validating its effectiveness and broad applicability.

A key innovation lies in the SS-Mix module, which generates augmented samples through intra-trial interpolation. Unlike existing GAN-based augmentation methods such as GANSER [19] and SA-cWGAN [20], which risk introducing low-quality or identity-inconsistent samples, SS-Mix explicitly preserves subject identity by avoiding inter-subject mixing. This design enhances intra-subject emotional variability while reducing semantic noise, thus improving model robustness and generalizability. To address the evolving nature of feature distributions, we introduce a dynamic distribution alignment strategy in RKHS, which jointly aligns both marginal and conditional distributions through multi-kernel MMD-based losses. Compared to fixed or marginal alignment approaches—such as BiHDM [34], MS-MDA [7], MS-FRAN [8], DA-CapsNet [35], SDDA [11], PR-PL [13] and DAPLP [10], our method offers finer-grained adaptation to inter-subject and inter-class shifts. Empirical results show that this component alone contributes to a 5.6% accuracy gain and reduces class-level feature overlap, as visualized in the t-SNE plots. Moreover, we propose a novel DSCL mechanism to overcome the limitations of contrastive learning approaches such as CLISA [15] and CL-CS [17], which rely on synchronized stimulus assumptions and suffer from poor generalization under asynchronous conditions. SDC-Net instead infers latent structural similarities within and across domains and selectively enforces consistency constraints without relying on time alignment or pseudo-labels. This enables robust learning of semantic boundaries, even in unlabeled target domains. Ablation experiments confirm that removing this module causes a 3–4% drop in performance, demonstrating its critical role in enhancing discriminability and transferability.

The ablation studies confirm that removing either the structure-aware consistency module or the dynamic reweighting mechanism leads to a 4%–6% performance degradation, highlighting the necessity of each component. Sensitivity analyses (Fig.7–8) further show that the model maintains high robustness under a wide range of kernel numbers and

similarity thresholds, with accuracy fluctuation consistently under 2%. Finally, the robustness of SDC-Net is further validated through visualization and sensitivity analyses. As shown in the t-SNE plots (Fig. 6), emotion categories form more compact clusters with reduced domain discrepancy. Moreover, hyperparameter studies (Fig.7-9) indicate that our method delivers consistently stable performance across a wide range of settings. To further highlight its reliability, we also investigate the risk of negative transfer—a known challenge in domain adaptation where transferred knowledge may impair target performance—and show that SDC-Net is highly resilient to such effects.

In the Future, several promising directions are deserved to research. Firstly, improving pseudo-label quality: One possible enhancement is adjusting the pseudo-label confidence threshold during the later stages of model training to ensure higher label quality. However, setting an excessively high threshold may discard too many uncertain pseudo-labels, leading to an imbalance between categories and low pseudo-label utilization [62], [63]. Therefore, future work should focus on optimizing the balance between the quantity and quality of pseudo-labels, potentially through adaptive thresholds or other robust filtering techniques. Another important avenue is the real-time deployment of the SDC-Net framework within an online aBCI system, facilitating dynamic user interaction. This would allow continuous model updates based on real-time EEG data, facilitating high-precision emotion recognition in dynamic, real-world settings. Testing and integrating our model into such an interactive online aBCI environment would provide a strong foundation for personalized emotion recognition systems that can adapt in real-time.

VI. CONCLUSION

This paper proposes a novel domain adaptation framework to address the challenge of individual variability in aBCIs for cross-subject EEG emotion recognition. The framework integrates three key innovations: SS-Mix data augmentation, dynamic distribution alignment in RKHS, and dual-domain similarity consistency learning Strategy. These components collectively enhance the generalization ability and robustness of emotion recognition models across different subjects.

Experimental results on the SEED, SEED-IV and FACED datasets demonstrate the superiority of the proposed framework in both cross-subject and cross-session scenarios, significantly improving emotion recognition performance. In future work, we plan to explore the integration of online transfer learning techniques to address real-world variability and enable real-time adaptation for practical applications.

REFERENCES

- [1] B. Hsueh, R. Chen, Y. Jo, D. Tang, M. Raffiee, Y. S. Kim, M. Inoue, S. Randles, C. Ramakrishnan, S. Patel *et al.*, “Cardiogenic control of affective behavioural state,” *Nature*, vol. 615, no. 7951, pp. 292–299, 2023.
- [2] D. J. Anderson and R. Adolphs, “A framework for studying emotions across species,” *Cell*, vol. 157, no. 1, pp. 187–200, 2014.
- [3] X. Si, H. He, J. Yu, and D. Ming, “Cross-subject emotion recognition brain–computer interface based on fnirs and dbjnet,” *Cyborg and Bionic Systems*, vol. 4, p. 0045, 2023.

[4] Z. Wan, R. Yang, M. Huang, N. Zeng, and X. Liu, "A review on transfer learning in eeg signal analysis," *Neurocomputing*, vol. 421, pp. 1–14, 2021.

[5] S. J. Pan and Q. Yang, "A survey on transfer learning," *IEEE Transactions on knowledge and data engineering*, vol. 22, no. 10, pp. 1345–1359, 2009.

[6] S. Pan, "Q.: A survey on transfer learning," *IEEE Transactions on Knowledge and Data Engineering*, vol. 22, no. 10, pp. 1345–1359, 2010.

[7] H. Chen, M. Jin, Z. Li, C. Fan, J. Li, and H. He, "Ms-mds: Multisource marginal distribution adaptation for cross-subject and cross-session eeg emotion recognition," *Frontiers in Neuroscience*, vol. 15, p. 778488, 2021.

[8] W. Li, W. Huan, S. Shao, B. Hou, and A. Song, "Ms-fran: a novel multi-source domain adaptation method for eeg-based emotion recognition," *IEEE Journal of Biomedical and Health Informatics*, 2023.

[9] J. Li, S. Qiu, C. Du, Y. Wang, and H. He, "Domain adaptation for eeg emotion recognition based on latent representation similarity," *IEEE Transactions on Cognitive and Developmental Systems*, vol. 12, no. 2, pp. 344–353, 2019.

[10] X.-C. Zhong, Q. Wang, R. Li, Y. Liu, S. Duan, R. Yang, D. Liu, and J. Sun, "Unsupervised domain adaptation with pseudo-label propagation for cross-domain eeg emotion recognition," *IEEE Transactions on Instrumentation and Measurement*, 2025.

[11] Z. Li, E. Zhu, M. Jin, C. Fan, H. He, T. Cai, and J. Li, "Dynamic domain adaptation for class-aware cross-subject and cross-session eeg emotion recognition," *IEEE Journal of Biomedical and Health Informatics*, vol. 26, no. 12, pp. 5964–5973, 2022.

[12] H. Zhang, T. Zuo, Z. Chen, X. Wang, and P. Z. Sun, "Evolutionary ensemble learning for eeg-based cross-subject emotion recognition," *IEEE Journal of Biomedical and Health Informatics*, 2024.

[13] R. Zhou, Z. Zhang, H. Fu, L. Zhang, L. Li, G. Huang, F. Li, X. Yang, Y. Dong, Y.-T. Zhang *et al.*, "Pr-pl: A novel prototypical representation based pairwise learning framework for emotion recognition using eeg signals," *IEEE Transactions on Affective Computing*, vol. 15, no. 2, pp. 657–670, 2023.

[14] R. Zhou, W. Ye, Z. Zhang, Y. Luo, L. Zhang, L. Li, G. Huang, Y. Dong, Y.-T. Zhang, and Z. Liang, "Eegmatch: Learning with incomplete labels for semisupervised eeg-based cross-subject emotion recognition," *IEEE Transactions on Neural Networks and Learning Systems*, 2024.

[15] X. Shen, X. Liu, X. Hu, D. Zhang, and S. Song, "Contrastive learning of subject-invariant eeg representations for cross-subject emotion recognition," *IEEE Transactions on Affective Computing*, vol. 14, no. 3, pp. 2496–2511, 2022.

[16] S. Dai, M. Li, X. Wu, X. Ju, X. Li, J. Yang, and D. Hu, "Contrastive learning of eeg representation of brain area for emotion recognition," *IEEE Transactions on Instrumentation and Measurement*, 2025.

[17] M. Hu, D. Xu, K. He, K. Zhao, and H. Zhang, "Cross-subject emotion recognition with contrastive learning based on eeg signal correlations," *Biomedical Signal Processing and Control*, vol. 104, p. 107511, 2025.

[18] L. Wang, S. Wang, B. Jin, and X. Wei, "Gc-stcl: A granger causality-based spatial-temporal contrastive learning framework for eeg emotion recognition," *Entropy*, vol. 26, no. 7, p. 540, 2024.

[19] Z. Zhang, Y. Liu, and S.-h. Zhong, "Ganser: A self-supervised data augmentation framework for eeg-based emotion recognition," *IEEE Transactions on Affective Computing*, vol. 14, no. 3, pp. 2048–2063, 2022.

[20] J. Chen, Z. Tang, W. Lin, K. Hu, and J. Xie, "Self-attention gan for eeg data augmentation and emotion recognition," *Computer Engineering and Applications*, vol. 59, no. 05, pp. 160–168, 2023.

[21] X. Du, X. Wang, L. Zhu, X. Ding, Y. Lv, S. Qiu, and Q. Liu, "Electroencephalographic signal data augmentation based on improved generative adversarial network," *Brain Sciences*, vol. 14, no. 4, p. 367, 2024.

[22] T. Hastie, S. Rosset, J. Zhu, and H. Zou, "Multi-class adaboost," *Statistics and its Interface*, vol. 2, no. 3, pp. 349–360, 2009.

[23] X.-W. Wang, D. Nie, and B.-L. Lu, "Emotional state classification from eeg data using machine learning approach," *Neurocomputing*, vol. 129, pp. 94–106, 2014.

[24] O. Bazgir, Z. Mohammadi, and S. A. H. Habibi, "Emotion recognition with machine learning using eeg signals," in *2018 25th national and 3rd international iranian conference on biomedical engineering (ICBME)*. IEEE, 2018, pp. 1–5.

[25] A. Craik, Y. He, and J. L. Contreras-Vidal, "Deep learning for electroencephalogram (eeg) classification tasks: a review," *Journal of neural engineering*, vol. 16, no. 3, p. 031001, 2019.

[26] Q. Yao, H. Gu, S. Wang, and X. Li, "A feature-fused convolutional neural network for emotion recognition from multichannel eeg signals," *IEEE Sensors Journal*, vol. 22, no. 12, pp. 11 954–11 964, 2022.

[27] W.-L. Zheng and B.-L. Lu, "Personalizing eeg-based affective models with transfer learning," in *Proceedings of the twenty-fifth international joint conference on artificial intelligence*, 2016, pp. 2732–2738.

[28] W. Samek, F. C. Meinecke, and K.-R. Müller, "Transferring subspaces between subjects in brain–computer interfacing," *IEEE Transactions on Biomedical Engineering*, vol. 60, no. 8, pp. 2289–2298, 2013.

[29] H. Zhang, "mixup: Beyond empirical risk minimization," *arXiv preprint arXiv:1710.09412*, 2017.

[30] W.-L. Zheng and B.-L. Lu, "Investigating critical frequency bands and channels for EEG-based emotion recognition with deep neural networks," *IEEE Transactions on Autonomous Mental Development*, vol. 7, no. 3, pp. 162–175, 2015.

[31] W. Zheng, W. Liu, Y. Lu, B. Lu, and A. Cichocki, "Emotionmeter: A multimodal framework for recognizing human emotions," *IEEE Transactions on Cybernetics*, pp. 1–13, 2018.

[32] J. Chen, X. Wang, C. Huang, X. Hu, X. Shen, and D. Zhang, "A large finer-grained affective computing eeg dataset," *Scientific Data*, vol. 10, no. 1, p. 740, 2023.

[33] P. Zhong, D. Wang, and C. Miao, "Eeg-based emotion recognition using regularized graph neural networks," *IEEE Transactions on Affective Computing*, vol. 13, no. 3, pp. 1290–1301, 2020.

[34] Y. Li, L. Wang, W. Zheng, Y. Zong, L. Qi, Z. Cui, T. Zhang, and T. Song, "A novel bi-hemispheric discrepancy model for eeg emotion recognition," *IEEE Transactions on Cognitive and Developmental Systems*, vol. 13, no. 2, pp. 354–367, 2020.

[35] S. Liu, Z. Wang, Y. An, B. Li, X. Wang, and Y. Zhang, "Da-capsnet: A multi-branch capsule network based on adversarial domain adaption for cross-subject eeg emotion recognition," *Knowledge-Based Systems*, vol. 283, p. 111137, 2024.

[36] Y. Li, W. Zheng, L. Wang, Y. Zong, and Z. Cui, "From regional to global brain: A novel hierarchical spatial-temporal neural network model for eeg emotion recognition," *IEEE Transactions on Affective Computing*, vol. 13, no. 2, pp. 568–578, 2019.

[37] Y. Gu, X. Zhong, C. Qu, C. Liu, and B. Chen, "A domain generative graph network for eeg-based emotion recognition," *IEEE Journal of Biomedical and Health Informatics*, vol. 27, no. 5, pp. 2377–2386, 2023.

[38] X. Yang, Z. Zhu, G. Jiang, D. Wu, A. He, and J. Wang, "Dc-astgcn: Eeg emotion recognition based on fusion deep convolutional and adaptive spatio-temporal graph convolutional networks," *IEEE Journal of Biomedical and Health Informatics*, 2024.

[39] H. Gao, X. Wang, Z. Chen, M. Wu, Z. Cai, L. Zhao, J. Li, and C. Liu, "Graph convolutional network with connectivity uncertainty for eeg-based emotion recognition," *IEEE Journal of Biomedical and Health Informatics*, 2024.

[40] W. Ye, Z. Zhang, F. Teng, M. Zhang, J. Wang, D. Ni, F. Li, P. Xu, and Z. Liang, "Semi-supervised dual-stream self-attentive adversarial graph contrastive learning for cross-subject eeg-based emotion recognition," *IEEE Transactions on Affective Computing*, 2024.

[41] C. Ren, J. Chen, R. Li, W. Zheng, Y. Chen, Y. Yang, X. Zhang, and B. Hu, "Semi-supervised pairwise transfer learning based on multi-source domain adaptation: A case study on eeg-based emotion recognition," *Knowledge-Based Systems*, vol. 305, p. 112669, 2024.

[42] J. Pan, R. Liang, Z. He, J. Li, Y. Liang, X. Zhou, Y. He, and Y. Li, "St-scgn: a spatio-temporal self-constructing graph neural network for cross-subject eeg-based emotion recognition and consciousness detection," *IEEE Journal of Biomedical and Health Informatics*, 2023.

[43] T. Song, W. Zheng, P. Song, and Z. Cui, "Eeg emotion recognition using dynamical graph convolutional neural networks," *IEEE Transactions on Affective Computing*, vol. 11, no. 3, pp. 532–541, 2018.

[44] J. Li, S. Qiu, Y.-Y. Shen, C.-L. Liu, and H. He, "Multisource transfer learning for cross-subject eeg emotion recognition," *IEEE transactions on cybernetics*, vol. 50, no. 7, pp. 3281–3293, 2019.

[45] W. Jiang, G. Meng, T. Jiang, and N. Zuo, "Generalization across subjects and sessions for eeg-based emotion recognition using multi-source attention-based dynamic residual transfer," in *2023 International Joint Conference on Neural Networks (IJCNN)*. IEEE, 2023, pp. 1–8.

[46] D. Pan, H. Zheng, F. Xu, Y. Ouyang, Z. Jia, C. Wang, and H. Zeng, "Msfr-gcn: A multi-scale feature reconstruction graph convolutional network for eeg emotion and cognition recognition," *IEEE Transactions on Neural Systems and Rehabilitation Engineering*, 2023.

[47] E. Zanaty, "Support vector machines (svms) versus multilayer perception (mlp) in data classification," *Egyptian Informatics Journal*, vol. 13, no. 3, pp. 177–183, 2012.

[48] J. J. Bird, J. Kobylarz, D. R. Faria, A. Ekárt, and E. P. Ribeiro, "Cross-domain mlp and cnn transfer learning for biological signal processing: Eeg and emg," *IEEE Access*, vol. 8, pp. 54 789–54 801, 2020.

[49] J. Wang, "Cross-subject domain adaptation study for eeg-based emotion recognition," *Neural Netw. Theory Appl.*, vol. 14, no. 8, pp. 1–7, 2022.

[50] Y. Ganin, E. Ustinova, H. Ajakan, P. Germain, H. Larochelle, F. Laviolette, M. March, and V. Lempitsky, "Domain-adversarial training of neural networks," *Journal of machine learning research*, vol. 17, no. 59, pp. 1–35, 2016.

[51] W. Li, L. Fan, S. Shao, and A. Song, "Generalized contrastive partial label learning for cross-subject eeg-based emotion recognition," *IEEE Transactions on Instrumentation and Measurement*, 2024.

[52] L. Breiman, "Random forests," *Machine learning*, vol. 45, pp. 5–32, 2001.

[53] D. Coomans and D. L. Massart, "Alternative k-nearest neighbour rules in supervised pattern recognition: Part 1. k-nearest neighbour classification by using alternative voting rules," *Analytica Chimica Acta*, vol. 136, pp. 15–27, 1982.

[54] J. A. Suykens and J. Vandewalle, "Least squares support vector machine classifiers," *Neural processing letters*, vol. 9, pp. 293–300, 1999.

[55] S. J. Pan, I. W. Tsang, J. T. Kwok, and Q. Yang, "Domain adaptation via transfer component analysis," *IEEE transactions on neural networks*, vol. 22, no. 2, pp. 199–210, 2010.

[56] B. Sun, J. Feng, and K. Saenko, "Return of frustratingly easy domain adaptation," in *Proceedings of the AAAI conference on artificial intelligence*, vol. 30, no. 1, 2016.

[57] B. Fernando, A. Habrard, M. Sebban, and T. Tuytelaars, "Unsupervised visual domain adaptation using subspace alignment," in *Proceedings of the IEEE international conference on computer vision*, 2013, pp. 2960–2967.

[58] H. Li, Y.-M. Jin, W.-L. Zheng, and B.-L. Lu, "Cross-subject emotion recognition using deep adaptation networks," in *Neural Information Processing: 25th International Conference, ICONIP 2018, Siem Reap, Cambodia, December 13–16, 2018, Proceedings, Part V 25*. Springer, 2018, pp. 403–413.

[59] Y. Ganin, E. Ustinova, H. Ajakan, P. Germain, H. Larochelle, F. Laviolette, M. March, and V. Lempitsky, "Domain-adversarial training of neural networks," *Journal of Machine Learning Research*, vol. 17, no. 59, pp. 1–35, 2016.

[60] Y. An, S. Hu, S. Liu, X. Wang, Z. Gu, and Y. Zhang, "Lgdaan-nets: A local and global domain adversarial attention neural networks for eeg emotion recognition," *Knowledge-Based Systems*, p. 113613, 2025.

[61] E. Harmon-Jones, P. A. Gable, and C. K. Peterson, "The role of asymmetric frontal cortical activity in emotion-related phenomena: A review and update," *Biological psychology*, vol. 84, no. 3, pp. 451–462, 2010.

[62] B. Zhang, Y. Wang, W. Hou, H. Wu, J. Wang, M. Okumura, and T. Shinnozaki, "Flexmatch: Boosting semi-supervised learning with curriculum pseudo labeling," *Advances in Neural Information Processing Systems*, vol. 34, pp. 18 408–18 419, 2021.

[63] Y. Wang, H. Chen, Q. Heng, W. Hou, Y. Fan, Z. Wu, J. Wang, M. Savvides, T. Shinnozaki, B. Raj *et al.*, "Freematch: Self-adaptive thresholding for semi-supervised learning," *arXiv preprint arXiv:2205.07246*, 2022.